Radio Science, Volume 33, Number 2, Pages 291–302, March–April 1998

Sea-air and boundary layer temperatures measured by a scanning 5-mm-wavelength radiometer: Recent results

Ed R. Westwater, Yong Han, Vladimir G. Irisov, and Vladimir Y. Leuskiy

Cooperative Institute for Research in Environmental Sciences, Environmental Technology Laboratory
Boulder, Colorado

Yuri G. Trokhimovski and Christopher W. Fairall

NOAA/ERL Environmental Technology Laboratory, Boulder, Colorado

Andrew T. Jessup

Applied Physics Laboratory, University of Washington, Seattle

Abstract. A scanning 5-mm-wavelength (60 GHz) radiometer was deployed during two recent experiments. The first was in September–October in 1995 when the Environmental Technology Laboratory conducted the Coastal Ocean Probing Experiment off the Oregon coast. During this experiment the scanning radiometer was deployed on the Floating Instrument Platform, a research vessel operated by the Scripps Institution of Oceanography. Ground truth for the radiometer was provided by two independent in situ and infrared measurements of the ocean surface temperature; ground truth for air temperature was also provided by two in situ measurements at 0.5 and 12 m above the ocean surface. The second experiment was during September 10–30, 1996, at the Department of Energy's Atmospheric Radiation Measurement Program's Cloud and Radiation Testbed site near Lamont, Oklahoma. Here ground truth for derived quantities consisted of 3-hourly radiosonde releases and measurements at 25 and 60 m from a meteorological tower. The results of the experiments indicate that the scanning radiometer yields accuracies of the order of 0.4°C rms for sea-air temperature difference and accuracies in temperature of better than 0.7°C rms at altitudes below 60 m.

1. Introduction

Several authors have reported on the importance of stability in determining the signatures of signals either scattered or emitted from the ocean surface. For example, stability has shown to be important for radar backscatter [*Keller et al.*, 1985; *Smirnov*, 1995] and for remote sensing of near-ocean surface wind speed by passive microwave polarimetry [*Pospelov*, 1996]. Finally, sea-air temperature difference has been shown to play a role in determining the statistics of sea surface mean-square slope, as measured by a scanning laser glint technique [*Shaw and Churnside*, 1997]. Conventionally, the sea-air temperature difference has been obtained by two separate instruments: one measuring the sea surface temperature (T_s) and the other measuring the air temperature. Measurements of the T_s can be made either by "bulk" methods, in which the temperature is measured from roughly 1 cm to several meters below the surface, or by infrared (IR) measurements of the so-called skin temperature [*Wick et al.*, 1996]. As Wick et al. point out, there can be a considerable difference between the two. The skin temperature is important for determining transport into the atmosphere because the surface is in direct contact with the air. Air temperature (T_a) is measured by an in situ sensor, usually placed about 10 m above the surface. However, whether bulk or IR measurements are used, the sea-air temperature difference ($\Delta T = T_s - T_a$) is determined by measurements from two sensors, each independently calibrated. The scanning 5-mm-wavelength radiometer [*Trokhimovski et al.*, 1998], which we describe in section 2, determines this temperature difference by relative measurements from the same instrument.

In atmospheric studies, low-level temperature gradients are also important to meteorology and air pollution studies. The gradients can be determined

Paper number 97RS02747.
0048-6604/98/97RS-02747$11.00

from radiosondes, released on a twice-daily basis at National Weather Service Field Office locations, or those released on an episodic basic for research purposes. In addition, several locations have instrumented towers, such as the Boulder Atmospheric Observatory, near Erie, Colorado, which has a 300-m tower, or the Department of Energy's Cloud and Radiation Testbed (CART) site, near Lamont, Oklahoma, which has a 60-m tower that is instrumented at two levels. Clearly, a small, easily deployable remote sensor, especially a passive one, could play an important role in boundary layer studies. Following a technique that was suggested by *Westwater* [1972], such passive microwave instruments have been developed in Russia [*Troitsky et al.*, 1993; *Trokhimovski et al.*, 1998] and are available commercially. Other techniques that we do not evaluate here include active virtual temperature soundings from radio acoustic sounding systems [*May et al.*, 1989] and passive infrared soundings from a Fourier transform infrared radiometer [*Revercomb et al.*, 1993].

In this paper we describe the deployment of a 5-mm-wavelength scanning radiometer (hereinafter referred to simply as a 5-mm radiometer) in two completely different field experiments, one devoted to ocean studies and the other to studies of water vapor in the atmosphere. However, they had one thing in common: Excellent sources of ground truth were available. The radiometer itself was built by and loaned to the Environmental Technology Laboratory (ETL) by the Lebedev Physical Institute of the Russian Academy of Sciences, Moscow, Russia, and is described by *Trokhimovski et al.* [1998].

2. Description of the 5-mm Scanning Radiometer

The 5-mm (60 GHz) radiometer was designed for precise, continuous measurements of sea-air temperature difference and for recovery of air temperature profiles (height from 0 to 300 m). This device was first used from a research vessel during the Joint U.S.-Russia Internal Waves Experiment (JUSREX) in July 1992 [*Trokhimovski et al.*, 1998]. A similar radiometer and technique was applied to atmospheric sounding by *Troitsky et al.* [1993]. The radiometer is a total power system with automatic compensation of the direct current in the output signal (a compensation-type radiometer). No additional modulation, except for the antenna beam rotation, is done in the radiometer. The scanning mirror of the radiometer rotates at 1.3 Hz. Details of the radiometer are shown in Table 1.

Table 1. Parameters of the 5-mm Scanning Radiometer

Parameter	Value
Total power compensation type	
Center frequency	60.5 GHz
Bandwidth	4 GHz
Beam width, 3 dB	6.6°
System noise temperature	1200 K
Sensitivity (rms @ 1 s)	0.025 K
Scan rate	1.3 Hz

The main idea of the radiometric technique is to measure oceanic and atmospheric emission in a wavelength band that exhibits relatively high atmospheric attenuation. Radiometric measurements are made in a scanning mode, and the radiometer measures brightness temperature relative to the air. In this case the radiation in the horizontal direction can be used as a reference level because the brightness temperature is nearly equal to the air temperature at the measurement height. For the two field experiments considered here, we used radiometric measurements at wavelengths near the peak of the 5-mm oxygen absorption band; multifrequency measurements in this band are commonly employed for recovery of atmospheric temperature profiles [*Troitsky et al.*, 1993; *Westwater*, 1993]. The oceanic data presented in section 4 confirm that the technique recovers sea-air temperature difference to an accuracy of about 0.4°C rms (or 5–7%) and can provide long, continuous observations. The technique is simple and can be used not only from a ship but also from low-altitude airborne platforms.

In addition to the sea-air temperature difference, the same measurements provide information about air temperature profiles in the lower atmosphere [*Troitsky et al.*, 1993; *Westwater*, 1972]. Thus it is possible to compare different parameters that are related to heat and momentum fluxes and to check predictions of surface layer models. We conclude that the proposed technique could be deployed widely in the investigation of ocean-atmosphere interactions.

3. The Coastal Oceans Probing Experiment (COPE)

3.1. Experiment, Site, and Instrumentation

During September–October 1995 the Environmental Technology Laboratory (ETL) organized the

Table 2. Coastal Ocean Probing Experiment Bulk Meteorological Data

Parameter	Unit	Instrument
T_a, ETL	°C	Vaisala HMP-35 thermistor on port boom (h = 12 m)
T_a, UW	°C	Sea-Bird SBE-3 oceanographic thermometers (h = 0.5 m)
T_s, ETL	°C	floating YSI thermistor
T_s, UW	°C	Sea-Bird SBE-3 oceanographic thermometers (z = 0.05 m)
Upward IR flux, ETL	W/m^2	Eppley pyrgeometer, downward facing
Downward IR flux, ETL	W/m^2	Eppley pyrgeometer, upward facing
Upward solar flux, ETL	W/m^2	Eppley pyranometer, downward facing
Downward solar flux, ETL	W/m^2	Eppley pyranometer, upward facing
T_s IR, ETL	°C	computed from IR flux, emissivity = 0.97
T_s IR, UW	°C	Heimann KT-19 radiation pyrometer (2° field of view)
Wind speed, ETL	m/s	Vector average wind from sonic anemometer
Wind direction, ETL	deg	Meteorological convention, assume FLIP pointed 300

Abbreviations are ETL, Environmental Technology Laboratory; UW, University of Washington; and FLIP, Floating Instrument Platform.

Coastal Ocean Probing Experiment (COPE) off the Oregon coast. The principal objectives of the study were to observe the signatures of the ocean surface with radars, lidars, and radiometers and to correlate these signatures with in situ measurements. The in situ observations were primarily taken from the Floating Instrument Platform (FLIP), a research vessel operated by the Scripps Institution of Oceanography. Microwave radiometric and polarimetric observations were taken from a blimp, while two microwave radiometers were operated on FLIP. Other blimp-mounted instruments included an X-band scatterometer, an altimeter, a Global Positioning System (GPS) receiver, and an IR thermal imager, all operated by the University of Washington. Of primary interest to this paper are the in situ instruments whose data are used for comparison with the 5-mm radiometer observations. A summary of relevant observations from FLIP is given in Table 2. The data are 10-min averages, and data from two sources for both air temperature and bulk sea temperature were taken. The IR measurements of skin temperature were made by two completely different techniques. The instrument used by ETL measured total hemispheric infrared flux from both upward and downward directions. From the difference of upward and downward flux, and with the assumption of emissivity =0.97, the sea surface temperature was derived. In addition, the downward facing ETL radiometers were operated looking up at the beginning and at the end of the experiment to cross calibrate with the regular upward facing instruments. The ETL radiative flux package was mounted near the end of the face boom at a distance of about 15 m from the hull. The face boom pointed roughly to the south, and the port boom, at right angles to the face boom, faced roughly to the west. The second IR instrument was the radiation pyrometer operated by the University of Washington (UW) and was mounted on the south side of the port boom at a distance of about 12 m from FLIP's main structure. It viewed the surface at an incidence angle of 15° and looked on the opposite side of the port boom from which the ETL scanning radiometer and infrared radiometers were facing.

The 5-mm radiometer was also mounted on the south side of the port boom at a distance about 10 m from FLIP's main structure. The altitude of the radiometer relative to the water surface was about 6 m. The flux-measuring packages of ETL, some of which are given in Table 2, were located at the end of the same boom. The UW measurements of bulk T_s (from a thermistor chain at depths ranging from 0.05 cm to 2 m) and T_a (h = 0.5 m) were made from the middle of the face boom. The geometry of the locations was such that all measurements were sampling areas of water within about 15 m of each other. One other geometrical consideration is important: With the wind coming from the easterly–northeasterly directions, all instruments could be looking at surfaces disturbed differently by the hull of FLIP.

Because we had two independent sets of measurements for each of the quantities T_s, T_a, and T_s IR, we could compare the measurements of $\Delta T(=T_s - T_a)$ by the 5-mm radiometers with several different values. Since the T_a and T_s measurements agreed well with each other, we formed composite values by averaging these bulk data when they coexisted and using the separate values when data from one of the sensors were not available. For the comparisons of the 5-mm radiometer with the IR, because the IR

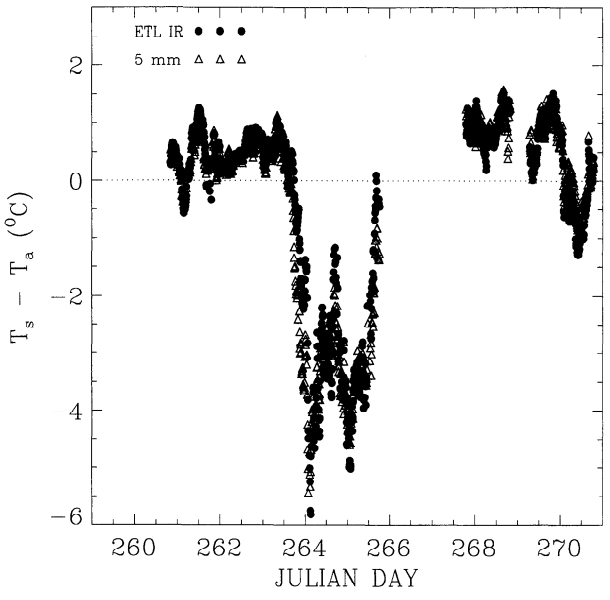

Figure 1. Time series of sea-air temperature difference as measured by the scanning 5-mm radiometer and by the Environmental Technology Laboratory (ETL) infrared radiometric measurements of T_s and composite T_a data. The data were obtained during the Coastal Ocean Probing Experiment (COPE) in September–October 1995.

measurements did not always agree well with each other, we compared only individual data sources.

3.2. Five-Millimeter Radiometer Measurement Technique and Calibration During COPE

The 5-mm radiometric measurements were performed with an instrument that was slightly modified from the one used during JUSREX. First, the local oscillator in the radiometer was shifted to a higher frequency. The total band was estimated as 58.5–62.5 GHz. Note that this shift of central frequency does not change the ocean skin depth, which is 0.3 mm [*Trokhimovski et al.*, 1998]. Next, the polarization of the radiometer was changed. During COPE the antenna received horizontal polarization (in JUSREX vertical polarization). Near nadir the water surface was observed at vertical polarization; at grazing angles it was observed at horizontal polarization. Such an installation provides better agreement between air temperature and brightness temperature in the horizontal direction.

The calibration of the radiometer output and antenna beam orientation was performed before COPE on the Boulder Atmospheric Observatory research tower [*Kaimal and Gaynor*, 1983] during August 18–19, 1995. Scale calibration was performed from five different tower altitudes: 10, 50, 100, 200, and 300 m. Radiometric measurements were accompanied by radiosonde measurements and direct measurement of air temperature from sensors on the tower platform. Comparisons between calculated and measured brightness temperatures were used for the determination of calibration coefficients.

3.3. Results From COPE

Preliminary retrievals of sea-air temperature difference, ΔT, were based on the brightness temperature measurements T_b at angles 48°–57° from nadir and with an averaging time of 12 min. A time series of ΔT from the 5-mm radiometer is shown in Figure 1. Also shown is the corresponding ΔT obtained by ETL IR and composite T_a measurements. In this plot the composite T_a is obtained from data described in rows 1 and 2 of Table 2, and ETL IR T_s is obtained from the data described in row 9. It is obvious from the figure that at least a qualitative agreement exists between the data sets. A plot showing similar agreement could be shown between the 5-mm data and those derived using the UW IR T_s measurements (T_s IR from the data in row 10) or from the various sets of bulk T_s and T_a data (rows 1–4). During COPE, both stable (air warmer than water) and unstable (air colder than water) conditions were encountered; for example, the data between Julian days 264 and 266 are stable. This change in stability was associated with winds coming from off the Oregon coast.

To evaluate the accuracy, or at least the precision, of our measurements, we prepared scatterplots between the 5-mm ΔT data and ΔT as derived from both the bulk and the IR methods. These scatterplots, as well as the regression lines of best fit, are shown in Figures 2 and 3 for the ETL and UW data. The regression fits were done using an algorithm that assumes that both variables are in error. We note that substantially better agreement is achieved between the 5-mm and the ETL IR method of determining ΔT than with either the UW IR or either of the bulk data. An agreement between microwave and IR was expected, since both the 5-mm and the IR radiometers measure T_s in the first few millimeters (or less) of the ocean surface, i.e., the skin layer. The skin depth of the 5-mm measurements is about 0.3 mm, while that of the IR data is about 10 μm. We note that the slope of the regression line is close to unity for 5-mm and ETL IR measurements, with an offset of about −0.08°C. The corresponding slope and offset for

5-mm and ETL bulk measurements is 0.84 and −0.09°C. However, the slope and offset comparisons with the UW data were not as close. To determine the cause of the slope discrepancies, we also did a scatterplot and regression analysis between ΔT determined from the ETL and UW bulk and IR measurements; see Figure 4. We note that there is a 20% difference in the slope between ETL and UW measurements. Additional analysis showed that the ETL and UW bulk T_s measurements differed by only 0.1°C rms and that the T_a measurements differed by 0.45°C rms. Thus the major difference was in the two separate measurements of infrared skin temperature, which differed by 0.52°C rms. Even more striking was the difference in their biases between stable and unstable conditions of 0.82°C.

The reasons for the differences between the two infrared measurements and the agreement between the ETL IR and microwave measurements have not been completely resolved. By far the largest difference between the two IR measurements occurred between days 264 and 266, a period associated with a change in stability from unstable to stable conditions. Furthermore, there was a substantial change in wind direction from 150° to 250° to nearly northerly–northeasterly (350°–360° and 0°–50°). The wind from offshore also was in a direction in which the hull of FLIP disturbed the flow of air to both the port and face booms. The disturbance of air flow also has an

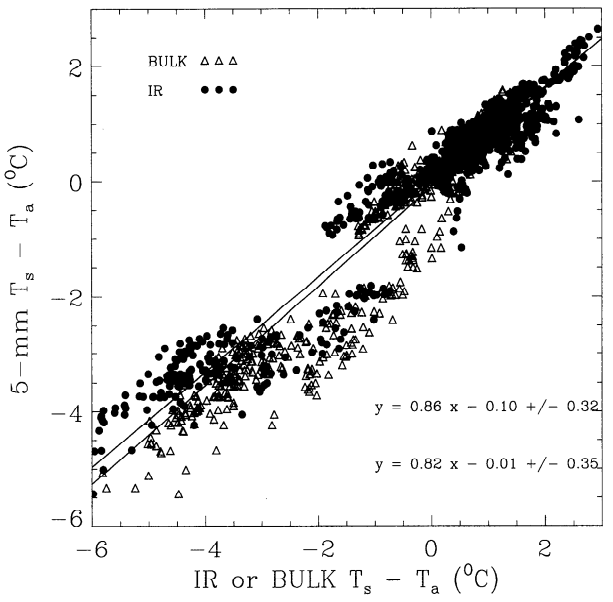

Figure 3. Same as Figure 2 but for University of Washington (UW) infrared data.

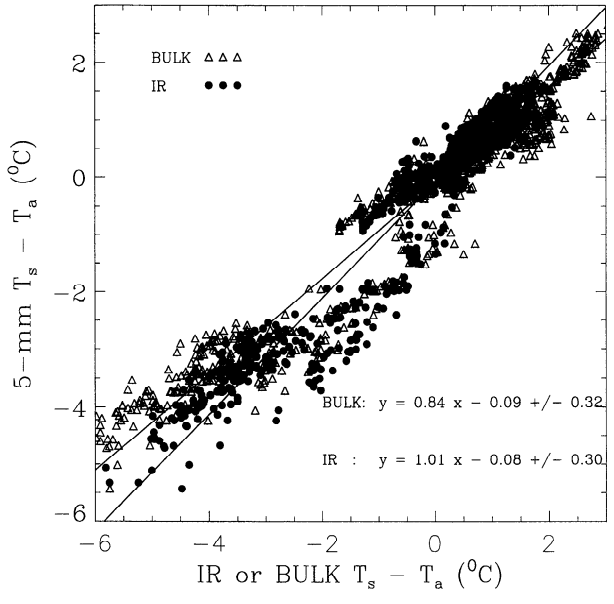

Figure 2. Scatterplots and regression lines of sea-air temperature difference as measured by the scanning 5-mm radiometer and by composite bulk and ETL infrared data. The data were obtained during COPE in September–October 1995.

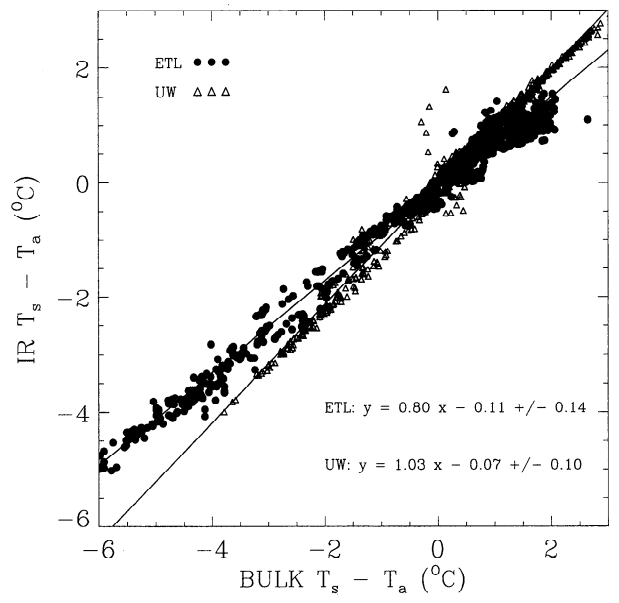

Figure 4. Scatterplots and regression line of sea-air temperature difference as measured by the ETL and UW infrared radiometers and by composite bulk data obtained at COPE in September–October 1995.

Table 3. Statistical Comparisons of Coastal Ocean Probing Experiment

Data Source	Offset, °C	Slope	Dispersion, °C	Rms, °C	Sample size
ΔT: ETL bulk versus 5-mm	−0.113	0.812	0.343	0.616	1086
ΔT: UW bulk versus 5-mm	−0.115	0.844	0.332	0.599	998
ΔT: ETL IR versus 5-mm	−0.011	1.018	0.304	0.431	1038
ΔT: UW IR versus 5-mm	−0.089	0.802	0.350	0.669	690
T_a: UW versus ETL	0.276	0.995	0.182	0.451	832
T_s: UW versus ETL	−0.322	1.023	0.101	0.160	795
T_s IR: UW versus ETL	−10.011	1.605	0.322	0.525	1104
ΔT: composite bulk versus 5-mm	0.094	0.835	0.321	0.569	1350

$\Delta T = T_s - T_a$.

impact on surface roughness. Independent measurements of skin temperature were also made by the UW's infrared imager during a controlled surface disruption experiment [*Schiff*, 1996], and these measurements indicated that the UW narrow field-of-view (FOV) measurements were correct. We believe that the most likely cause of error in the 5-mm radiometric measurements, if they are in error, would be the influence of the hull on the spectrum of ocean waves determining microwave emissivity. The UW narrow FOV technique is considered to be more accurate than the ETL technique, which is based on differences of total hemispheric upward and downward irradiance. Nevertheless, it is intriguing that the ETL 5-mm and infrared measurements agree so well. A summary of regression comparisons between all of these data is given in Table 3. The overall differences between the measurements are less than 0.7°C rms. If we assume statistical independence between 5-mm and bulk determinations, we get $E(\Delta T_{5\text{-mm}} - \Delta T_{\text{bulk}})^2 = E(\Delta T_{5\text{-mm}})^2 + E(\Delta T_s)^2 + E(\Delta T_a)^2$, where E refers to average or expectation value over an ensemble of measurements. Evaluating the error budgets from the numbers given in Table 3 for 5-mm versus composite bulk determination, we get $E(\Delta T_{5\text{-mm}})^2 = E(\Delta T_{5\text{-mm}} - \Delta T_{\text{bulk}})^2 - E(\Delta T_s)^2 - E(\Delta T_a)^2 = (0.408°\text{C})^2$. Thus we estimate the error in the 5-mm measurements as about 0.4°C rms.

We also derived the air temperature gradient from 10 to 50 m from the upper part of the 5-mm radiometric scan (Figure 5); the retrieval method is outlined by *Trokhimovski et al.* [1998]. In general, our data allow us to retrieve the air temperature profile in the layer 0–300 m. Note that the air temperature gradient has good correlation with ΔT derived from the both portions of 5-mm measurements and with in situ measurements (Figure 1). Again, we used an averaging time of 12 min to provide about the same time resolution as the in situ measurements. Ground truth for the air temperature gradient was not available during COPE; however, excellent verification data were available for the second experiments described in this paper, and comparisons are given in section 5.3.

4. Radiometric Observations at the Southern Great Plains Cloud and Radiation Testbed (CART) Site

4.1. Experiment, Site, and Instrumentation

As a part of the Department of Energy's Atmospheric Radiation Measurement (ARM) Program, a comprehensive measurement facility has been developed in the Southern Great Plains of north central Oklahoma and south central Kansas [*Stokes and Schwartz*, 1994]. The central facility of this Cloud and Radiation Testbed (CART) site is located near Lamont, Oklahoma. A variety of in situ and remote

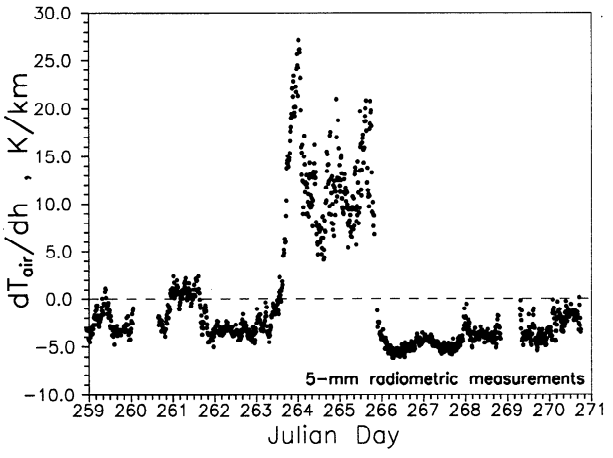

Figure 5. Time series of air temperature gradient between the surface and 50 m as measured by the scanning 5-mm radiometer data obtained at COPE experiment in September–October 1995.

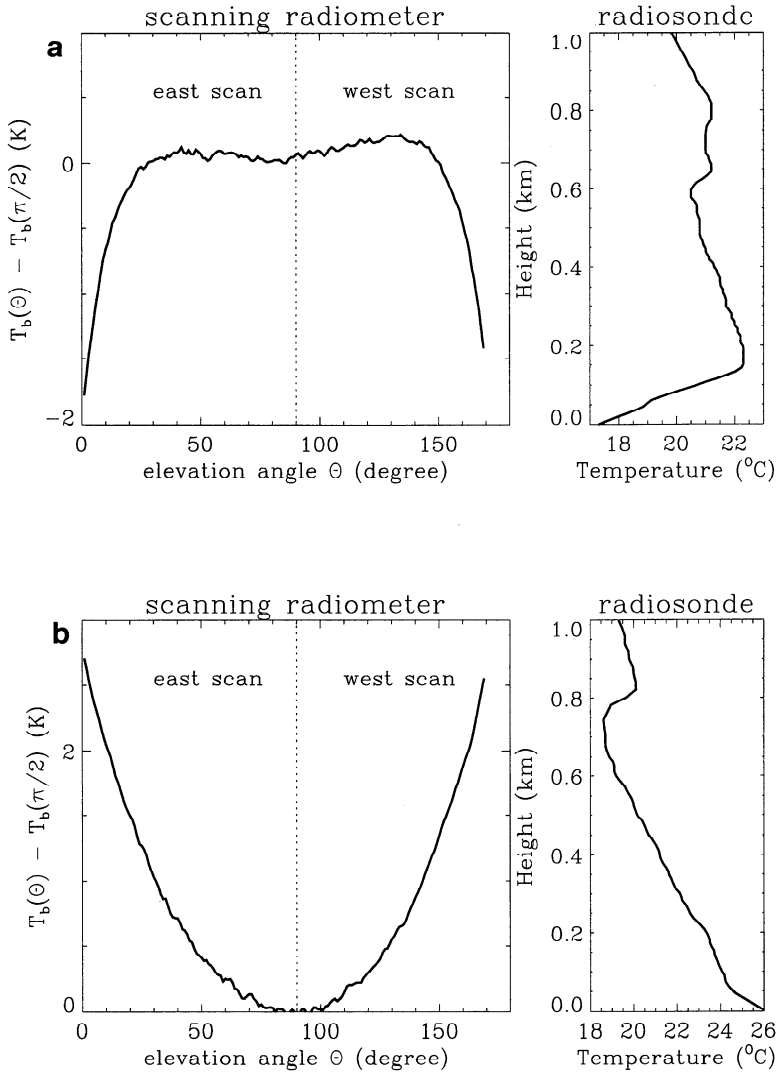

Figure 6. $T_b(\theta) - T_b(\pi/2)$ for the 5-mm scanning radiometer and the corresponding radiosonde sounding of temperature for (a) a ground-based thermal inversion and (b) lapse conditions. The elevation angle $\theta = \pi/2$ corresponds to zenith. The observations were made at the Southern Great Plains (SGP) Cloud and Radiation Testbed (CART) site in September 1996.

meteorological sensors, as well as radiation sensors, are routinely operated at this central facility. During September 10–30, 1996, an intensive operating period (IOP) was conducted at this facility. The IOP, although focused primarily on measurements of water vapor, also provided an excellent set of data for temperature.

We operated the scanning 5-mm radiometer from the top northeast edge of a seatainer (3 m above ground level (AGL)) that housed an ETL water vapor radiometer. The radiometer performed a complete 360° scan in the east-west direction. Data obtained from the upper portion of the scan were used to derive temperature gradients; observations from the lower portion of the scan were of a shallow valley containing grass to the east and a plowed field to the west. At times, nonsymmetric scan patterns were suggestive of differences in solar heating on the two different surfaces.

Temperature ground truth for the radiometer was obtained from two sources: 3-hourly radiosonde releases from a location about 200 m to the north from

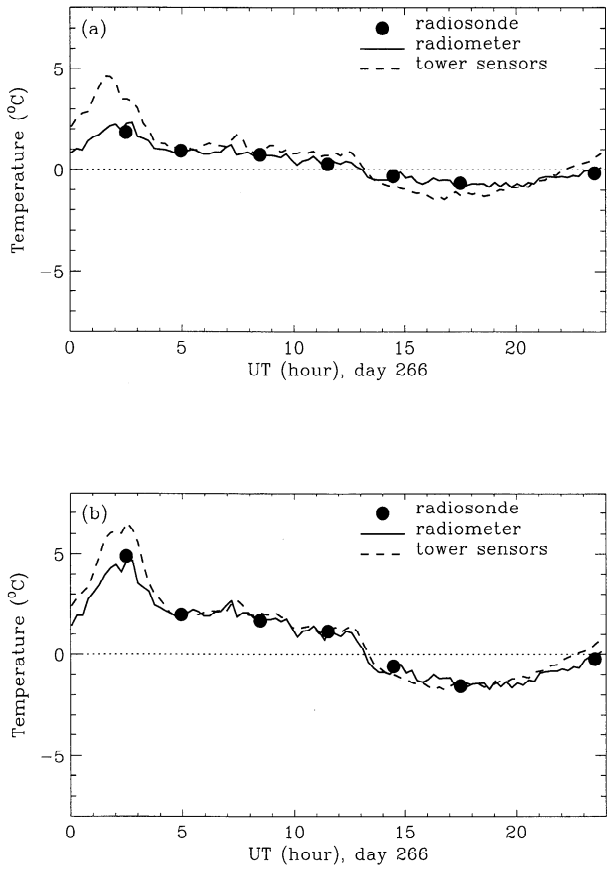

Figure 7. Time series of differences in air temperature at two levels measured at the SGP CART site by three sensors on Julian day 266 in September 1996: (a) temperature (25 m) − temperature (surface) and (b) temperature (60 m) − temperature (surface). The 5-mm west scan was used because that direction was closest to the tower.

the radiometer and from tower measurements (about 40 m to the south) of temperature. The tower contained instruments that measured both temperature and humidity at 25 and 60 m AGL. The tower was at about the same altitude as the radiometer, and both were about 4 m higher than the radiosonde release site (the standard meteorological shelter was at 2 m AGL). Thus, for comparisons between air temperature measurements and using the CART surface meteorological station as a reference for surface data, relative altitudes are 5 m for the 5-mm radiometer and 27 and 62 m for the tower.

4.2. Five-Millimeter Radiometer Calibration and Retrieval Technique Used at the CART Site

Calibration of the radiometer was done using a one-parameter adjustment. This parameter was determined by a least squares comparison of measured and calculated brightness temperatures for 160 radiosonde soundings of temperature as a function of height. The calculations were performed using *Liebe*'s [1989] microwave propagation model. In these comparisons for elevation angles that covered a range of 2.5°–90°, both the radio frequency band pass and the antenna power pattern were taken into account.

The method for the temperature lapse rate retrieval was a modification of linear statistical inversion [*Westwater*, 1993]. We assembled a 20-year ensemble of radiosonde data from the Oklahoma City, Oklahoma, area. We then computed T_b as a function of frequency and elevation angle θ and averaged them over the band pass and antenna pattern of the radiometer (see Table 1). Gaussian noise of 0.1 K rms was added to the measurements. We then retrieved the relative temperature difference between T(60 m) and T(4 m) and between T(25 m) and T(4 m) as a function of T_b difference: $\Delta T_b = T_b(\theta) - T_b(\pi/2)$. For economy of representation, we projected the measured ΔT_b on the first four empirical orthogonal functions and used this projection as our (four-component) data vector.

4.3. Comparisons of Radiometric Retrievals With in Situ Data at the CART Site

Examples of raw 5-mm radiometer data and radiosonde observations are shown in Figure 6. Figure 6a shows observations during a ground-based thermal inversion. Note that T(150 m) is about 5°C warmer than the surface. The corresponding ΔT_b is about 2 K. Figure 6b shows a lapse condition with a near-adiabatic lapse rate in the first 50 m above the ground. Here ΔT_b is about 3 K and with a significantly different sign and signature from the inversion case. We also note in Figure 6a a slight east-west asymmetry that we believe comes from a nonstratified thermal environment.

Figures 7, 8, and 9 show time series plots of radiometrically retrieved, tower, and radiosonde values of the difference in temperature between the tower and the surface at the two tower levels. As mentioned in section 4.1, the surface values were made at a standard meteorological shelter. Here we selected the west scan for the radiometric comparisons because this direction was closest to the tower. In general, the correspondence between all measurements is reasonable, considering the spatial differences between the sensors. In Figure 7, there is closer agreement between the radiometer and the radio-

sonde than with the tower. In Figure 8 the agreement is mixed, with the radiometer sometimes agreeing better with the radiosonde and sometimes better with the tower. Figure 9 shows a day that was entirely overcast, and hence the diurnal heating pattern was completely absent. Here all data are in excellent agreement. Thus it seems apparent that the relatively small differences that do occur are the result of spatial inhomogeneity in the temperature field.

We also computed the temperature from the radiometer for both the east and the west scan versus the temperature from the tower sensors, as shown in Figures 10 and 11. Here we see substantial differences between the scans during the day. Remembering that the west scan is closest to the tower and that substantial differences between surface heating occur during the day, the results are quite suggestive that lack of horizontal stratification is a major reason for the radiometer-tower differences. We consider the rms differences of about 0.7 K, achieved on the west scan, to be quite respectable.

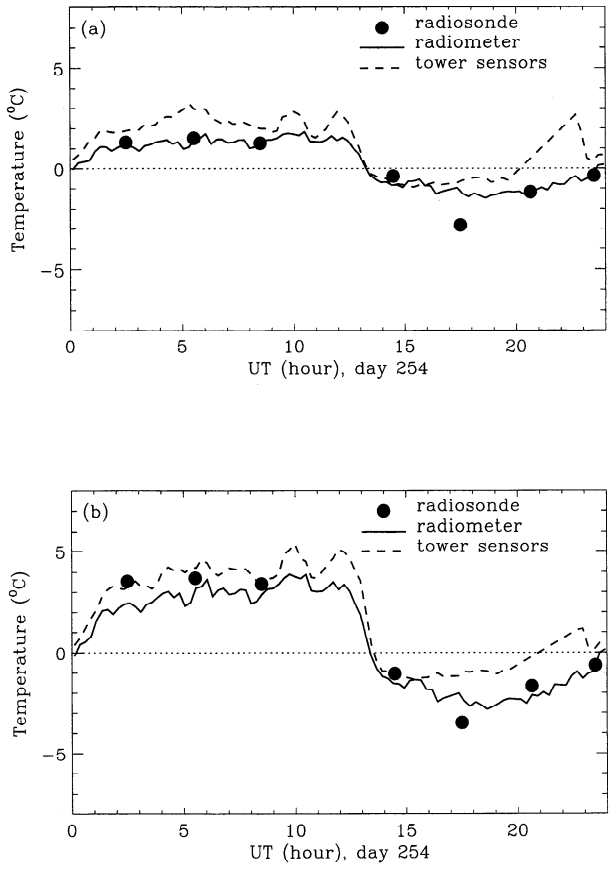

Figure 8. Same as Figure 7 but for Julian day 254.

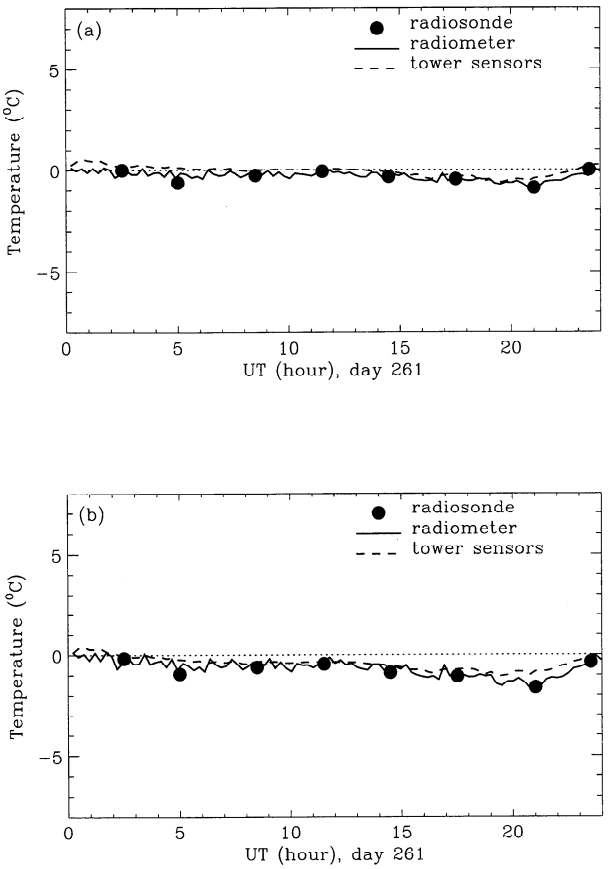

Figure 9. Same as Figure 7 but for Julian day 261.

These results become even more impressive if radiosonde and tower measurements are compared. In Figure 12, both the difference in temperature between 25 m and the surface and between 60 m and the surface are compared for the radiosonde versus the tower. In both cases the rms differences are substantially poorer than those between the radiometer and the tower. This is surely a result of the lack of horizontal homogeneity of the temperature field. For this reason we did not use radiosonde soundings to judge the accuracy of the radiometric boundary layer retrievals in the 100- to 300-m altitude range.

5. Summary and Conclusions

We evaluated the performance of a rapidly scanning 5-mm wavelength radiometer in two widely different environments. In the first we compared radiometric soundings of sea-air temperature differ-

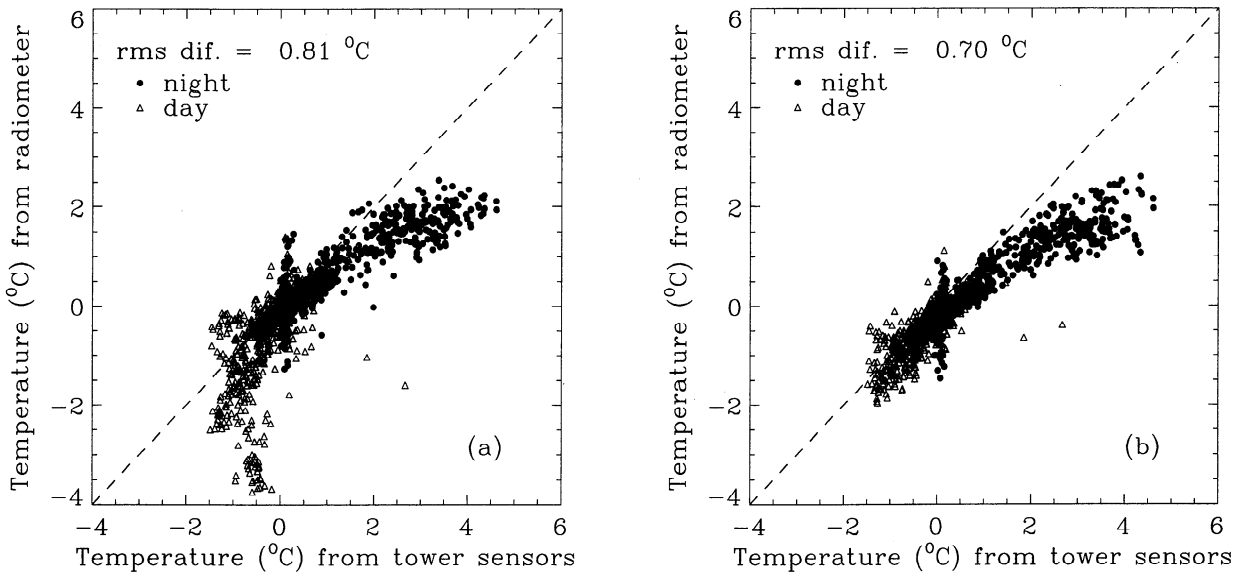

Figure 10. Scatterplots of temperature difference between 25 m and the surface as derived from the (a) east and (b) west scans of the 5-mm radiometer and the tower sensor data taken at the SGP CART site in September 1996.

ence with a variety of in situ measurements that were available on FLIP: two sets of T_a, two sets of T_s, and two sets of T_s IR. Here the differences between the 5-mm radiometric retrievals and other sets of data were less than 0.7°C rms. If we assume statistical independence of the various error sources, these results translate to a 0.4°C rms estimate for the accuracy of the 5-mm measurements. We also showed that there were substantial differences between two types of IR measurements of T_s. These differences can largely be attributed to the differences between the narrow FOV technique of UW versus the hemi-

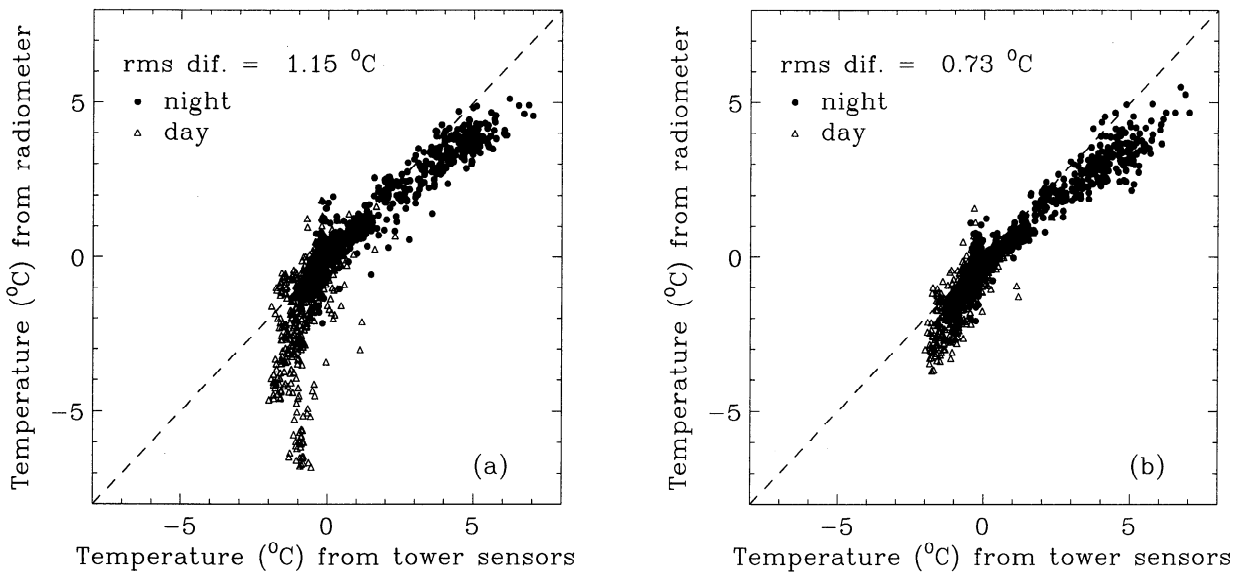

Figure 11. Same as Figure 9 but between 60 m and the surface.

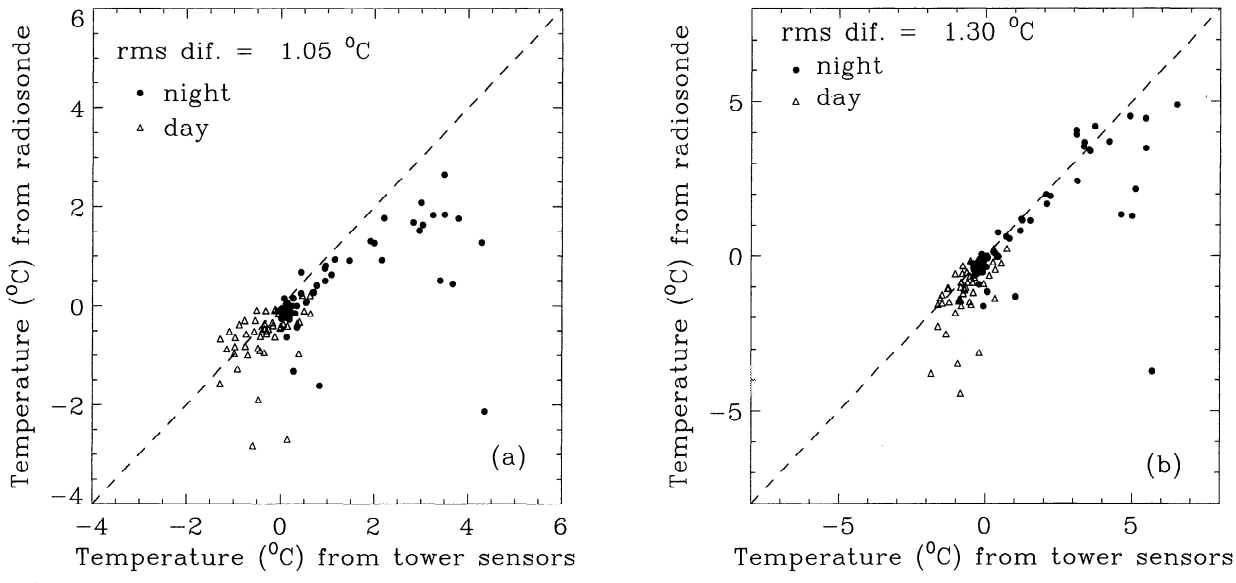

Figure 12. Scatterplots of temperature difference (a) between 25 m and the surface and (b) between 60 m and the surface as derived from radiosonde and the tower sensor data taken at the SGP CART site during September 1996.

spheric irradiance differencing technique of ETL. The largest difference between all of the measurements occurred during stable conditions associated with offshore flow; the hull of FLIP also blocked the airflow during these conditions. For situations in which blockage can be avoided, we believe that the accuracy of the 5-mm technique will exceed 0.4°C rms. Thus, the 5-mm radiometer, because of its simplicity and ruggedness, could be a useful addition to oceanographic research measurement. Because of the evaluation given in this paper, ETL has constructed its own 5-mm scanning radiometer.

In the second environment, that of the Southern Great Plains central Oklahoma CART site, excellent agreement (rms differences of 0.7°C) was found between the radiometer and measurements at 25- and 60-m levels of a meteorological tower. These results are in good agreement with those of previous investigators [*Troitsky et al.*, 1993]. The agreement with the tower was substantially better than that of nearby radiosondes. It was found that substantial differences existed between temperatures derived from scans to the west and those to the east. Thus some information on horizontal thermal gradients is also available from this instrument. The instrument could be easily deployed for air pollution studies and in environments where knowledge of low-altitude temperature gradients is important. Since the deployment of towers is difficult, at best, and radiosondes may not always yield reliable measurements in the first few tens of meters, we suggest that scanning 5-mm radiometers could be useful in research and monitoring. A commercial version of this instrument is available in Russia, and one of the Russian units will be deployed at the ARM site at the North Slope of Alaska.

Acknowledgments. This study was partially supported by the Advanced Sensor Applications Program of the U.S. Department of Defense and by the Environmental Sciences Division of the Department of Energy as a part of their Atmospheric Radiation Measurements Program. The work was done while Y. G. Trokhimovski held an NRC-NOAA/ERL/ETL research associateship. We also acknowledge the helpful comments of E. N. Kadygrov and useful discussions with G. Wick and Joseph A. Shaw.

References

Kaimal, J. C., and J. E. Gaynor, The Boulder Atmospheric Observatory, *J. Clim. Appl. Meteorol.*, *22*(5), 863–880, 1983.

Keller, W. C., W. J. Plant, and D. E. Weissman, The dependence of X-band microwave sea return on atmospheric stability and sea state, *J. Geophys. Res.*, *90*(C1), 1019–1029, 1985.

Liebe, H. J., MPM—An atmospheric millimeter-wave propagation model, *Int. J. Infrared Millimeter Waves*, *10*, 631–650, 1989.

May, P. T., K. P. Moran, and R. G. Strauch, The accuracy of RASS temperature measurements, *J. Appl. Meteorol.*, *28*, 1329–1335, 1989.

Pospelov, M. N., Surface wind speed retrieval using passive microwave polarimetry: The dependence on atmospheric stability, *IEEE Trans. Geosci. Remote Sens.*, *34*(5), 1166–1171, 1996.

Revercomb, H. E., H. Buijs, R. G. Dedecker, T. P. Dirks, R. A. Herbsleb, R. O. Knuteson, J. F. Short, and W. L. Smith, Atmospheric emitted radiance interferometer (AERI) for ARM, in *Fourth Symposium on Global Change Studies*, pp. 46–49, Am. Meteorol. Soc., Boston, Mass., 1993.

Schiff, R. K., Calibrated field measurements of the effect of wind induced surface roughness on infrared sea surface temperature (SST), Masters thesis, 179 pp., Dep. of Civil Eng., Univ. of Wash., Seattle, 1996.

Shaw, J. B., and J. H. Churnside, Scanning-laser glint measurements of sea-surface mean-square slope, *Appl. Opt.*, *36*(18), 4202–4213, 1997.

Smirnov, A. V., Sea radar backscattering and instabilities in the ocean-atmosphere system, *NOAA Tech. Memo. ERL ETL-256*, 44 pp., NOAA Environ. Technol. Lab., Boulder, Colo., 1995.

Stokes, G. M., and S. E. Schwartz, The Atmospheric Radiation Measurement (ARM) Program: Programmatic background and design of the cloud and radiation testbed, *Bull. Am. Meteorol. Soc.*, *75*(7), 1201–1221, 1994.

Troitsky, A. V., K. P. Gaykovich, V. D. Gromov, E. N. Kadygrov, and A. S. Kosov, Thermal sounding of the atmospheric boundary layer in the oxygen absorption band center at 60 GHz, *IEEE Trans. Geosci. Remote Sens.*, *31*(1), 116–120, 1993.

Trokhimovski, Y. G., E. R. Westwater, Y. Han, and V. Y. Leuskiy, The results of air and sea surface temperature measurements using a 60 GHz microwave rotating radiometer, *IEEE Trans. Geosci. Remote Sens.*, *36*(1), 3–15, 1998.

Westwater, E. R., Ground-based determination of low altitude temperature profiles by microwaves, *Mon. Weather Rev.*, *100*(1), 15–28, 1972.

Westwater, E. R., Ground-based microwave remote sensing of meteorological variables, in *Atmospheric Remote Sensing by Microwave Radiometry*, edited by Michael A. Janssen, pp. 145–213, John Wiley, New York, 1993.

Wick, G. A., W. J. Emery, and P. Schlussel, The behavior of the bulk-skin sea surface temperature difference under varying wind speed and heat flux, *J. Phys. Oceanogr.*, *26*(10), 1969–1988, 1996.

C. W. Fairall and Y. G. Trokhimovski, NOAA/ERL Environmental Technology Laboratory, R/E/ET1, 325 Broadway, Boulder, CO 80303-3328. (e-mail: cfairall@etl.noaa.gov)

Y. Han, V. G. Irisov, V. Y. Leuskiy, and E. R. Westwater, Cooperative Institute for Research in Environmental Sciences, Environmental Technology Laboratory, R/E/ET1, 325 Broadway, Boulder, CO 80309-3328. (e-mail: yhan@etl.noaa.gov; virisov@ctl.noaa.gov; vleuskiy@etl.noaa.gov; ewestwater@etl.noaa.gov)

A. T. Jessup, Applied Physics Laboratory, University of Washington, Seattle, WA 98105-6698. (e-mail: jessup@apl.washington.edu)

(Received March 27, 1997; revised September 8, 1997; accepted September 30, 1997.)